Front. Earth Sci.
https://doi.org/10.1007/s11707-019-0804-6

RESEARCH ARTICLE

Determination of the crustal structure and seismicity of the Linfen rift with S-wave velocity mapping

Zigen WEI[1], Risheng CHU (✉)[1], Meiqin SONG[2], Xiaolin YANG[3], Shanshan WU[4], Feng BAO[1]

1 State Key Laboratory of Geodesy and Earth's Dynamics, Innovation Academy for Precision Measurement Science and Technology, Chinese Academy of Sciences, Wuhan 430077, China
2 Earthquake Administration of Shanxi Province, Taiyuan 030021, China
3 Shaanxi Earthquake Agency, Xi'an 710068, China
4 Shanghai Earthquake Agency, Shanghai 200062, China

Abstract The Linfen rift is a Cenozoic extensional rift with significant seismicity and seismic hazards. Studies of this rift shed light on deep dynamic processes and seismogenic mechanisms relevant to crustal structure and seismic activity. We first conducted a joint inversion of receiver functions and surface wave dispersion on waveform data collected from 27 broadband seismic stations to image the crustal S-wave velocity in the Linfen rift and its surroundings. We then relocated the source parameters for 10 earthquake events with depths > 20 km and studied the relationship between crustal S-wave velocity and seismicity. The results show that low-velocity zones of different scales exist in the middle-lower crust, and that the depth of the seismogenic layer gradually increases from ~25 km in the south to ~34 km in the north, roughly corresponding to the bottom of the low-velocity zone. We found that most of the relocated earthquakes occurred in the low-velocity zone at depths of 18 km to 34 km, with the deepest at 32 km. Two of the greatest historic earthquakes, Linfen (Ms 7.75) in 1695 and Hongtong (Ms 8.0) in 1303, occurred at the bottom of the high-velocity zone at depths of 12 km to 18 km. Our results, combined with previous studies, suggest that the upwelling mantle material below the rift did not remarkably affect the velocity structure from the bottom of the seismogenic layer down to the uppermost mantle nor heat the crust. It is likely that neither crustal-scale faults nor mantle earthquakes exist in the Linfen rift.

Keywords Linfen rift, joint inversion, S-wave velocity, seismogenic layer, deep crustal earthquake

Received April 30, 2019; accepted October 10, 2019

E-mail: chur@apm.ac.cn

1 Introduction

Rift zones represent an important component of the plate tectonic system which strongly influences the tectonic and dynamic characteristics of their surroundings. For example, Si et al. (2013) proposed that lithospheric delamination occurred beneath the Baikal Rift, which was caused by the collision between the Siberia Plate and the Mongolia-North China Plate during the Mesozoic. This delamination induced an upwelling of asthenospheric material and promoted the development of the rift. In addition, deep crustal earthquakes often occur in rifts due to their complex, deep structure, and special tectonic backgrounds, which thus provide a valuable opportunity to study their seismogenic environment. For instance, earthquakes have occurred at twice the depth of the Moho in the Rwenziori zone of the East African Rift, and are thought to be related to crustal delamination (Lindenfeld and Rümpker, 2011). Furthermore, abundant active faults exist in rifts, which often cause strong earthquakes accompanied by heavy casualties and property loss. For example, the Huaxian earthquake (Ms = 8.3), which struck the southern edge of the Shaanxi-Shanxi rift in 1556 CE, caused more than 830,000 deaths (Fig. 1) (Ma et al., 2016). The study of a rift's structure and seismogenic mechanisms can offer important information for mitigating the results of disastrous earthquakes. Likewise, studies of rift zones can provide both scientific and social value.

The characterization of seismogenic mechanisms in intra-plate earthquakes is a core objective of seismology. It is generally believed that most earthquakes occur in the upper-middle crust because the lower crust and upper mantle are generally too ductile and hot to accumulate the strain required for an earthquake (Ding and Zeng, 1990; Zhu et al., 2005; Zheng and Xie, 2017).

In recent years, improvements in sensors and processing have enabled seismologists to detect a growing number of intra-plate earthquakes (Yang et al., 2003; Wei et al., 2009; Cai et al., 2014) which appear to occur in the lower crust. Intra-plate earthquakes that occur in the upper mantle have also been observed in some areas, such as the Tibetan Plateau (Zhu and Helmberger, 1996; Chen and Yang, 2004; Jiang et al., 2009), the Hawaiian Islands (Wolfe et al., 2003), the Baikal Rift (Radziminovich et al., 2003), and the East African Rift (Lindenfeld and Rümpker, 2011). The discovery of these earthquakes has prompted a shift in our understanding of lithospheric rheological structure and seismogenic mechanisms in the lower crust and upper mantle.

The Linfen rift is located at the center of the S-shaped Shaanxi-Shanxi rift (Fig. 1), which was formed by the counterclockwise rotation of the Ordos Block along pre-existing weak zones caused by the collision between the North China Craton and the Tibetan Plateau (Zhang et al., 2003). A series of discontinuous normal faults with an NNE strike were established during the formation of the Linfen rift, accompanied by strong neotectonic movement and faulting activities (Xi and Zhang, 1977; Wang, 2000; Cai et al., 2014). The Linfen rift is a pure-shear and extensional rift, and shows similar shallow and deep structural characteristics to the Rwenziori region in the East African Rift. Earthquakes occur in the mantle, striking surface subsidence, local thinning of the crust, and lower seismicity velocity in the upper mantle (Zhao et al., 2009; Tang et al., 2010; Jiang et al., 2013).

Seismicity is active in the Linfen rift zone. Six strong earthquakes of $Ms > 6.0$ have occurred in since 649 CE, including a magnitude 8.0 that struck Hongtong (HT) in 1303 CE and a magnitude 7.75 that occurred in Linfen (LF) in 1695 CE (Ma, 1993; Gao, 1995; Shen et al., 2004). Presently, more than 200 small earthquakes occur each year. Recent seismicity studies have also detected numerous deep crustal earthquakes, even approaching the depth of the Moho (Song et al., 2012; Dong et al., 2013).

Numerous geophysical and geological studies have been done in the Linfen rift zone in recent years. The rift was formed during the Cenozoic (Zhang et al., 2003), with a relatively high surface heat flow (Hu et al., 2000) and more than 2 km of Cenozoic sediment (Xu et al., 1993). Based on the results from seismic exploration (Li et al., 2006; Li et al., 2014a) and earthquake data (Ren et al., 2012; Wei et al., 2015a), the crustal thickness is generally lower than 40 km, with an uplift of 3–6 km, and a topography that approximately mirrors that of the basin basement in the Linfen rift zone. Low-velocity anomalies extend from the top of the upper mantle to the mantle transition zone, as determined by the study of surface-wave and body-wave tomography (Zhao et al., 2009; Li et al., 2012; Jiang et al., 2013).

An increasing number of studies of the seismicity in the Linfen rift zone have been published in recent years (Hu et al., 2002; Yang et al., 2003; Jin et al., 2008; Song et al., 2012; Dong et al., 2013; Cai et al., 2014; Li et al., 2015a; Xu et al., 2018). These investigations have provided valuable information about source parameters and related seismogenic mechanisms. Small and moderate earthquakes in the Linfen rift were relocated by absolute and relative relocation methods between 1981 and 2008 (Song et al., 2012). These results show that most of these earthquakes occurred in the upper- and middle crust, while others occurred at a depth ranging from 30–40 km. Dong et al. (2013) reported similar results after relocating earthquakes from 1981 to 2010 using a double-difference location method. It was then speculated that there were crustal-scale faults in the Linfen rift zone. However, the focal depths of these deep crustal earthquakes remain controversial due to poor station coverage, a lack of stations located within a short epicentral distance, and low-resolution velocity models (Li et al., 2015b). Consequently, further validation and study of these deep crustal earthquakes is warranted.

In this paper, we conducted the joint inversion of receiver function and surface wave dispersion to image the crustal S-wave velocity in the Linfen rift using data collected from 27 broadband stations. Ten deep crustal earthquakes were then relocated using above crustal S-wave velocity information. Based on the high-resolution S-wave velocity structure and relocation results obtained in this study, we further analyze and discuss the tectonic evolution process and related seismogenic mechanism and environment in the Linfen rift.

2 Data and methods

2.1 Data

Teleseismic data from 20 temporary seismic stations (Fig. 1) used to extract receiver function were from the Seismic Array Laboratory, Institute of Geology and Geophysics, Chinese Academy of Sciences (Chen et al., 2014; Lou et al., 2017). These stations operated for 12–18 months with 10–20 km station spacing. The data from seven permanent stations (Fig. 1), recorded between 2012 and 2014, were from the Data Management Centre of China National Seismic Network, Waveform data of China National Seismic Network, Institute of Geophysics, and the China Earthquake Administration (Zheng et al., 2010). These data, with 30°–90° epicentral distances and > 5.5 magnitudes, were used to estimate the radial receiver functions by an iterative deconvolution method in time-domain (Herrmann, 2013).

Dispersion curves of surface wave phase velocity in different stations were observed from different results. Using stations numbered between 320 and 332 (Fig. 1), curves of 5–19 s, 31–60 s, and 20–30 s periods were calculated using ambient noise tomography (Ling et al., 2017), surface wave tomography (Wei et al., 2015b), and their average, respectively (Fig. 2). The phase velocity dispersion curves from the 8–50 s periods for the other

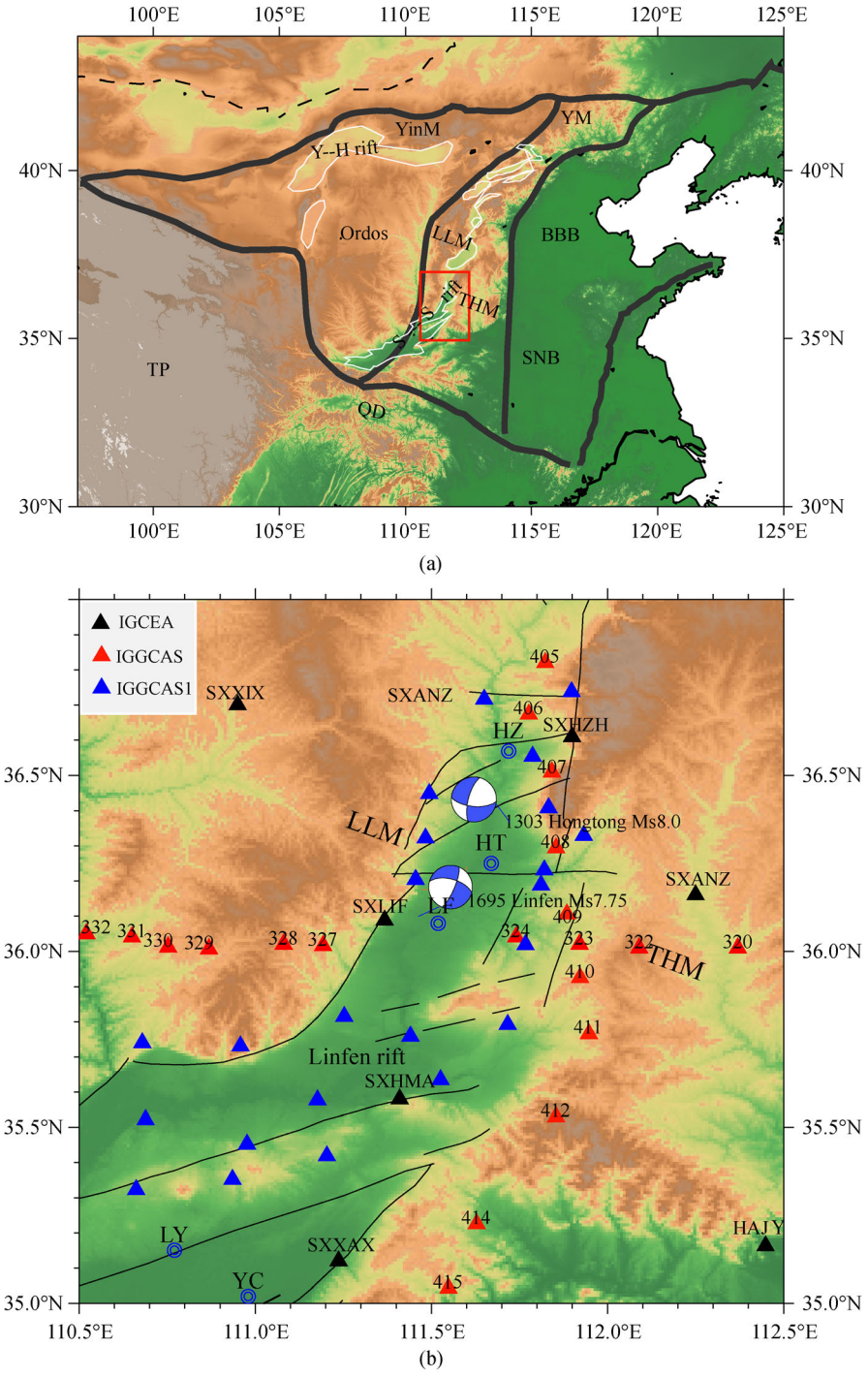

Fig. 1 Regional geological tectonic setting, active faults, broadband (red and black triangles) and short-period (blue triangles) and two strong earthquakes (Li et al., 2015a) in the Linfen rift. QD: Qinling-Dabie Orogen; TP: Tibetan Plateau; YinM: Yin Mountains; YM: Yan Mountains; LLM: Lüliang Mountains; THM: Taihang Mountains; S–S rift: Shaanxi–Shanxi rift; Y–H rift: Yinchuan–Hetao rift; Ordos: Ordos Block; SNCB: South North China Basin; BBB: Bohai Bay Basin; HZ: Huozhou City; HT: Hongtong City; LF: Linfen City; LY: Linyi City; YC: Yuncheng City; IGGCAS: Institute of Geology and Geophysics, Chinese Academy of Sciences; IGCEA: Institute of Geophysics, China Earthquake Administration; IGGCAS1: Institute of Geodesy and Geophysics, Chinese Academy of Sciences.

stations were taken from surface wave dispersion data (Shen et al., 2016).

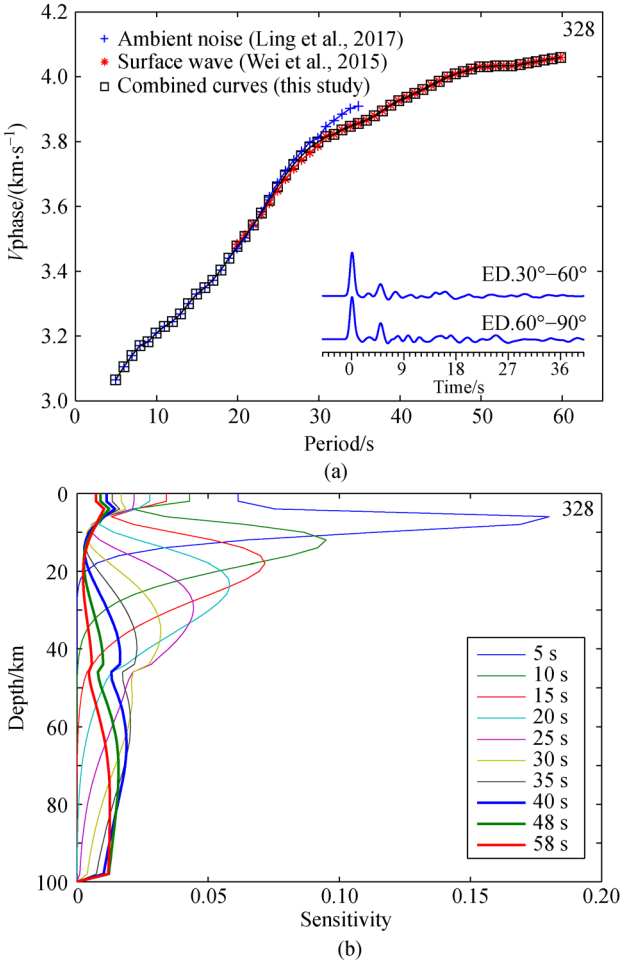

Fig. 2 Stacked receiver functions for 30°–60° and 60°–90° epicentral distances (ED.) and the surface wave dispersion curves (a). Phase velocity sensitivity kernels for shear velocity for different periods (b).

Relocation data from 23 short-period seismic stations for 10 earthquakes having focal depths of > 20 km, published by the China Earthquake Datacenter, are from the State Key Laboratory of Geodesy and Earth's Dynamics, Institute of Geodesy and Geophysics, and the Chinese Academy of Sciences. These stations were operated in November 2017 with 10–40 km station spacing.

2.2 Methods

2.2.1 Joint inversion of receiver function and surface wave dispersion

A receiver function is a waveform sequence in a time domain that results after disruptive factors from the seismic source factor, propagation path of the seismic wave, and instrument response, etc., have been removed. Receiver functions are widely used to image the crustal-mantle discontinuity and crustal velocity structure (Langston, 1977; Wu and Zeng, 1998; Chu et al., 2010; Feng et al., 2017). However, receiver functions have an inherent non-uniqueness and are typically unable to reveal accurate velocity information in an area with thick sediments and complex crustal structure. The surface wave is universally used to invert the absolute S-wave velocity structure in the crust and upper mantle (Shapiro and Campillo, 2004; Yao et al., 2006; Bao et al., 2013) because of its dispersion feature. Nevertheless, surface wave dispersion is insensitive to the interface of velocity and represents the total propagation effect of the travel path. The joint inversion of the receiver function and surface wave dispersion may bridge the resolution gaps and reduce the non-uniqueness of the inversion associated with each individual data set; therefore, this approach has been commonly applied to invert the crust-mantle velocity structure in recent years (Julià et al., 2000; Hu et al., 2005; Liu et al., 2014).

In this paper, we use joint inversion of the receiver function and surface wave dispersion with a Gaussian factor of 2.0 to image the crust-mantle velocity structure (Fig. 3). The weighting factors for the receiver function and the surface wave dispersion calculations were set to 0.5 and 0.5, respectively, for stations 320–332 in the joint inversion. The weighting factors of the receiver function and surface wave dispersion were set to 0.7 and 0.3, respectively, for other stations, due to the 50-km resolution of the surface wave dispersion (Shen et al., 2016). The inverted time-window for the receiver function was from-5 s to 40 s for all stations. Using the CRUST 1.0 model (Laske et al., 2013) and crustal thickness from the H-k stacking method of receiver function as an initial model (Wei et al., 2013, 2016), we applied a global optimizing approach for waveform inversion of receiver functions to obtain the S-wave velocity for five layers beneath each station (Li et al., 2010). Then, taking the S-wave velocity model as the new initial model, we used the joint inversion method to invert the S-wave velocity up to 70 km deep based on the sensitivity kernels of phase velocity for shear velocity for different periods (Fig. 2(b)).

2.2.2 Earthquake relocation

We used the typical seismic location code of HYPOINVERSE-2000 (Klein, 2007) to relocate the 10 earthquakes with focus depths of > 20 km and a magnitude ranging from 0.2 to 1.7 because of the good station coverage and stations with short epicentral distances for these events. For each earthquake recorded by at least four stations, the weighting values were set the same for P and S phases. We divided the study region into the northern and southern parts by the 36°N parallel based on the tectonic characteristics. According to the results from joint inversion herein, we considered the S-wave velocity from a location of 111.8°E and 36.5°N as well as

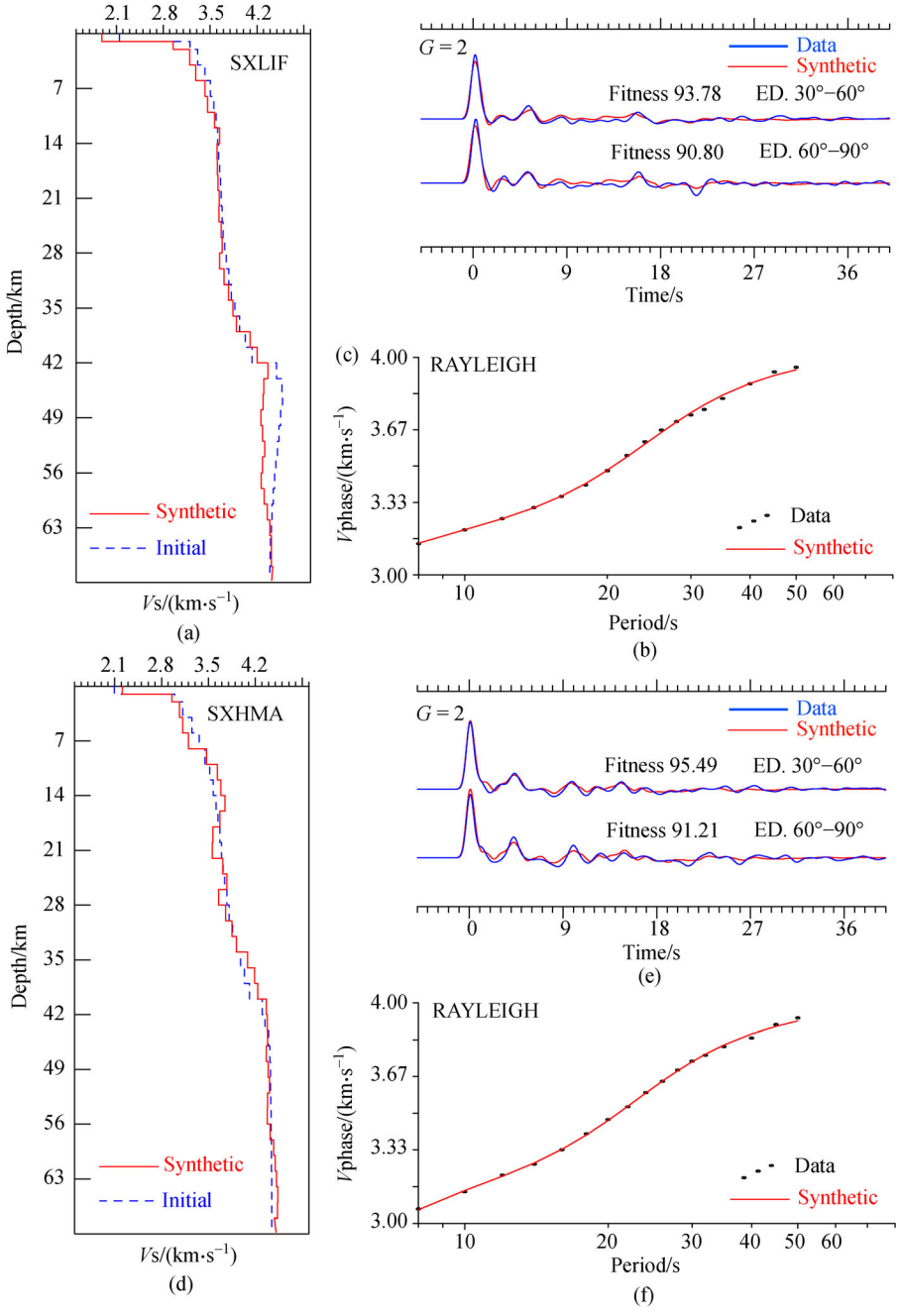

Fig. 3 Waveforms and results for typical stations by joint inversion method. G: Gaussian factor; ED: Epicentral distance.

110.5°E and 35.0°N as the initial model in the northern and southern regions, respectively (Figs. 4(a) and 4(b)). The initial model of P-wave velocity was 1.78 times of S-wave velocity (Zandt and Ammon, 1995).

3 Results and discussion

3.1 The S-wave velocity in the Linfen rift zone

Figure 3 shows the waveform characteristics and inverted results for two typical stations by the joint inversion method. The degree of fit for the receiver functions for different epicentral distances and dispersion curves of surface waves are all over 90%, indicating the relative reliability of these results. We studied the effect of uncertainty from initial models with 5% variations of velocity and data by adding random Gaussian noise within a 5% deviation for receiver functions and a 1% variation for dispersion curves on inverted S-wave velocities. The results show that the inverted S-wave velocities are insensitive to different initial models, and show similar patterns of velocity variation with depth to the corresponding final inverted models.

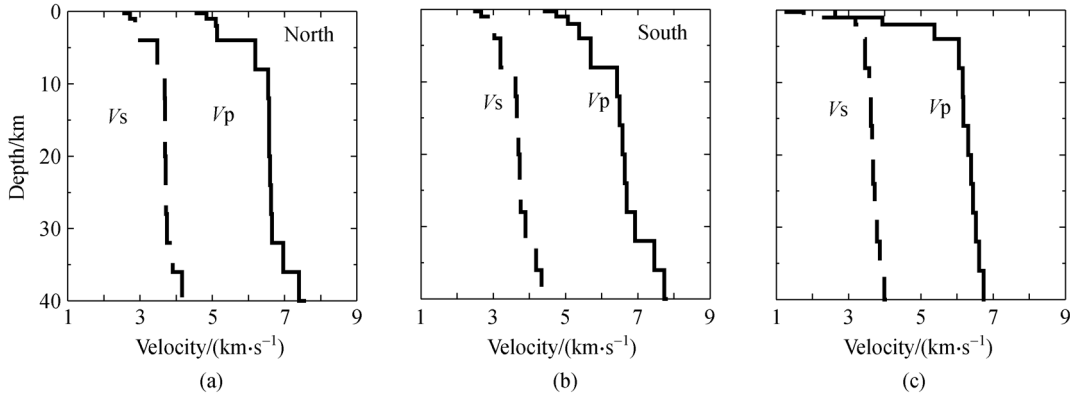

Fig. 4 Plots of the S- and P-wave velocity models used for joint inversion in the Linfen rift. Two S-wave velocity models (a, b) are the results of the joint inversion in this study, while the third (c) is obtained from the surface-wave dispersion result (Shen et al., 2016). P-wave velocities were assumed to be 1.78 times the S-wave velocities using joint inversion in our study (a, b) and the result of seismic exploration (c, Duan et al., 2016).

Figure 5 exhibits the S-wave velocities at different depths and across two profiles, as obtained by the joint inversion method in our study region. Changes in the velocity over small scales were found at different depths. There were pronounced differences in the S-wave velocities between the Linfen rift and the surrounding mountains at certain depths. At a depth of 2 km (Fig. 5(a)), obvious lower velocities were imaged in the cities of Huozhou (HZ), Yuncheng (YC), Linfen (LF), and Hongtong (HT), which is consistent with previous results from surface wave tomography and seismic exploration (Li et al., 2014b; Shen et al., 2016). At an 8-km depth (Fig. 5(b)), the S-wave velocity in the Linfen rift was lower than that in the Taihang Mountains (THM) or the Lüliang Mountains (LLM). At a 16-km depth (Fig. 5(c)), the S-wave velocity in the Linfen rift was higher than in the THM. Finally, at depths of 24 km, 32 km, 40 km, and 50 km, the differences in S-wave velocity between the Linfen rift and the surrounding mountains were marginal.

We noticed that the velocity was significantly lower in the middle crust beneath the W-E profile (Fig. 5(h)) than below the mountains. This region of lower velocity extends deeper in the Linfen rift, which is consistent with the ambient noise tomography results along this profile (Ling et al., 2017). Small-scale regions of lower velocity were also revealed in the middle-lower crust along the N-S profile (Fig. 5(i)). The connectivity and integration of these lower velocity regions were weaker in the Linfen rift than in the surrounding mountains. The lower-velocity and high-conductivity layer in the middle-lower crust beneath the Linfen rift and the adjacent THM (Figs. 5(h) and 5(i)) was also observed by the study of ambient noise tomography, seismic exploration, and magnetotelluric sounding (Tang et al., 2013; Li et al., 2014b; Yin et al., 2017), suggesting that the results of our joint inversion are reliable. Studies relying on the long-period surface wave tomography and body-wave tomography (Zhao et al., 2009; Jiang et al., 2013) observed distinctively lower velocity anomalies at depths ranging from the uppermost mantle to ~300 km in the Linfen rift. No lower velocity anomalies were imaged between the Moho and uppermost mantle beneath the Linfen rift, based on short-period surface wave and ambient noise tomography (Tang et al., 2013; Shen et al., 2016; Ling et al., 2017). In addition, no lower velocity anomalies were observed from the bottom of the lower crust to a depth of 70 km below the Linfen rift.

These observations suggest that the mantle materials below the rift zone may have little effect on the crust, even though the Moho was uplifted by 2–3 km. High surface heat flow (Hu et al., 2000), low gravity anomalies, and negative isostatic anomalies (Ma, 1993) have been noted in the Linfen rift zone, which may be related to the lower-velocity anomalies in the upper mantle which is typically accompanied by locally high temperatures. The lower-velocity body in the upper mantle may supply the heat to the middle and lower crust, which could explain the observed phenomena in addition to some of the crustal lower-velocity anomalies observed in our study. The small-scale velocity anomalies in the middle-lower crust are able to effectively concentrate local stress, which induces earthquakes.

3.2 Relocation results

Figure 6, Table 1, and Table 2 show the relocation results of ten earthquakes in 2017. The epicentral distances were relocated by an error of about 3 km or less, except for one earthquake (327/08:11:52) which was changed by ~6 km. The errors in the focus depth were less than 5 km in 70% of the earthquakes. This small error reinforced the reliability of the source parameters supplied by the China Earthquake Data Center. The stations used to relocate two typical

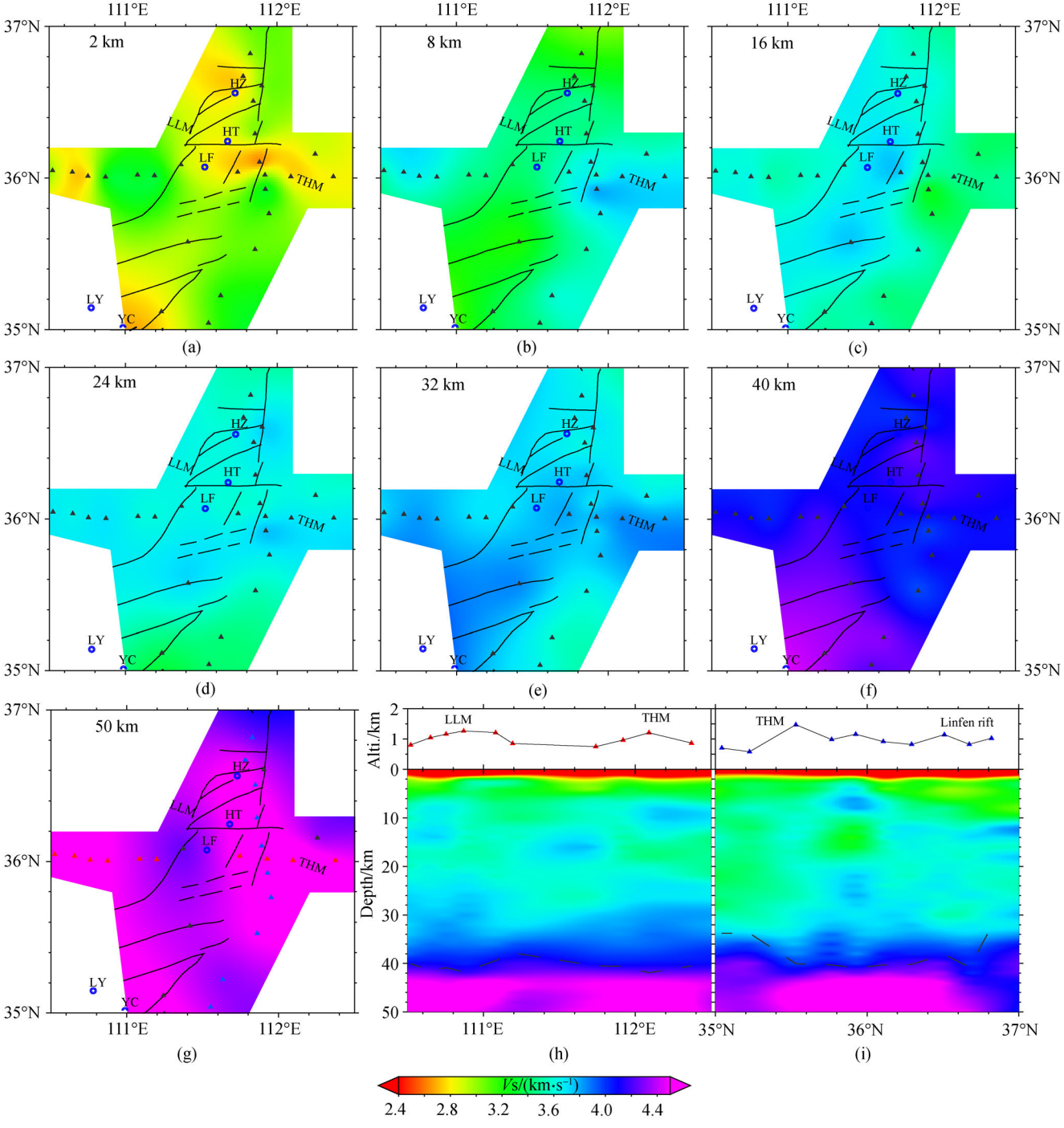

Fig. 5 The S-wave velocity distribution at different depths (a–g) in the study region and beneath two profiles (h–i). The profile locations are shown in g. Dashed lines (h, i) show the Moho (Wei et al., 2016). LLM: Lüliang Mountains; THM: Taihang mountains; HZ: Huozhou City; HT: Hongtong City; LF: Linfen City; LY: Linyi City; YC: Yuncheng City; Alti: Altitude.

earthquakes (336/03:11:00 and 317/10:48:45) are shown in Fig. 7, indicating good station coverage with relatively small epicentral distances. The focus depth differences for these two earthquakes were reduced to less than 1 km by exchanging the initial models, changing the weighting values for P- and S-wave phases, and were unreliable for partial stations (336/03:11:00 stations HZH and LIF and S8, 317/10:48:45 stations S16 and HMA and S23). One earthquake (336/03:11:00) occurred in the lower crust with a focus depth of 32 km. We applied different S-wave and P-wave models (Fig. 4) to evaluate the uncertainty in the earthquake's parameters and found that all calculated focus

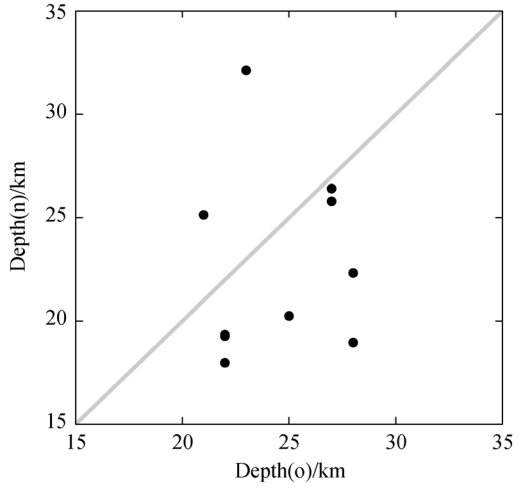

Fig. 6 The earthquake depths before and after relocation for ten deep earthquakes. The letters o and n indicate data from before and after relocation, respectively.

depths were deeper than 30 km (Fig. 6(a)). Previous studies suggest that the arrival time based method can achieve greater focus depth measurements (Mori, 1991) when the epicentral distance is less than 1.4 times the focus depth. The epicentral distances for most stations in this study were less than 1.4 times the focal depth of 32 km (Fig. 7(d)), with distances of 5 km, 14 km, 23 km, 26 km, 27 km, and 46 km for stations S2, SXHZH, S8, S5, S3 and S7, respectively. These tests and short epicentral distances point to the reliability of the relocations for these ten earthquakes and lend credibility to the finding that one earthquake (336/03:11:00) occurred in the lower crust.

3.3 Crust velocity vs. seismicity

Figure 8 shows the distribution of 1482 earthquakes with magnitudes of 0–5.0 occurring between February 1981 and August 2009. These earthquakes were relocated by absolute and relative relocating methods (Song et al., 2012), including those with poor reliability for focus depths > 30 km, due to poor station coverage and long epicentral distances to stations. The results show that most earthquakes occurred in the interior of the Linfen rift zone, and throughout the crust. These earthquakes, combined with the ten events relocated in this study, and two additional large historical earthquakes (Dong et al., 2013), were projected on two linear profiles of the S-wave velocity through the rift. The result indicates no relationship between magnitude and focus depth. The bottom boundary of focus distribution in the Linfen rift gradually declines from 25 km to 34 km in the S-N direction, roughly corresponding to the bottom of the lower velocity body in the middle and lower crust (Fig. 8(c)). This trend is consistent with the development characteristics from SW to NE, with the topography in the southwest becoming increasingly narrow in the northeast. An uneven lower-velocity zone with a depth between 18 km and 34 km,

Table 1 The original and relocation source parameters of ten earthquakes in 2017

Ear.(time)	Lon.(o)	Lat.(o)	Lon.(n)	Lat.(n)	Dep.(o)/km	Dep.(n)/km	Dep.(e)/km	ML.	N.(sta)
308/16:25:20	111.76	36.51	111.77	36.51	27.0	26.40	0.7	0.2	5
315/13:24:46	111.85	36.22	111.86	36.24	28.0	18.95	1.1	0.5	7
317/10:48:45	110.55	35.07	110.58	35.06	22.0	19.34	2.0	1.5	9
321/18:33:50	111.73	36.31	111.73	36.32	27.0	25.79	1.0	0.9	12
324/05:23:50	111.74	35.35	111.73	36.34	28.0	22.32	1.3	0.4	5
325/11:31:57	111.69	36.20	111.71	36.21	25.0	20.25	1.0	0.4	8
327/08:11:52	110.81	35.46	110.86	35.43	21.0	25.14	3.4	0.5	4
331/21:52:14	111.14	35.70	111.15	35.71	22.0	19.26	1.4	1.0	10
335/00:40:31	111.67	36.24	111.67	36.25	22.0	17.98	1.2	1.7	17
336/03:11:00	111.81	36.48	111.80	36.51	23.0	32.13	1.1	0.7	8

The letters o, n, and e in (a) indicate data from before relocation, after relocation, and the depth error, respectively (N.: Number, ML.: Local magnitude)

Table 2 Test results of focus depth for different velocity models (Fig. 4) in the Linfen rift

Earthquake	*V*s	*V*p	Dep./km	Dep.(e)/km
336/03:11:00	a	a	32.13	1.1
336/03:11:00	b	b	31.98	1.1
336/03:11:00	c	c	32.47	1.3
336/03:11:00	a	c	34.33	1.3
336/03:11:00	b	c	32.24	1.6

The letter e indicates the depth error

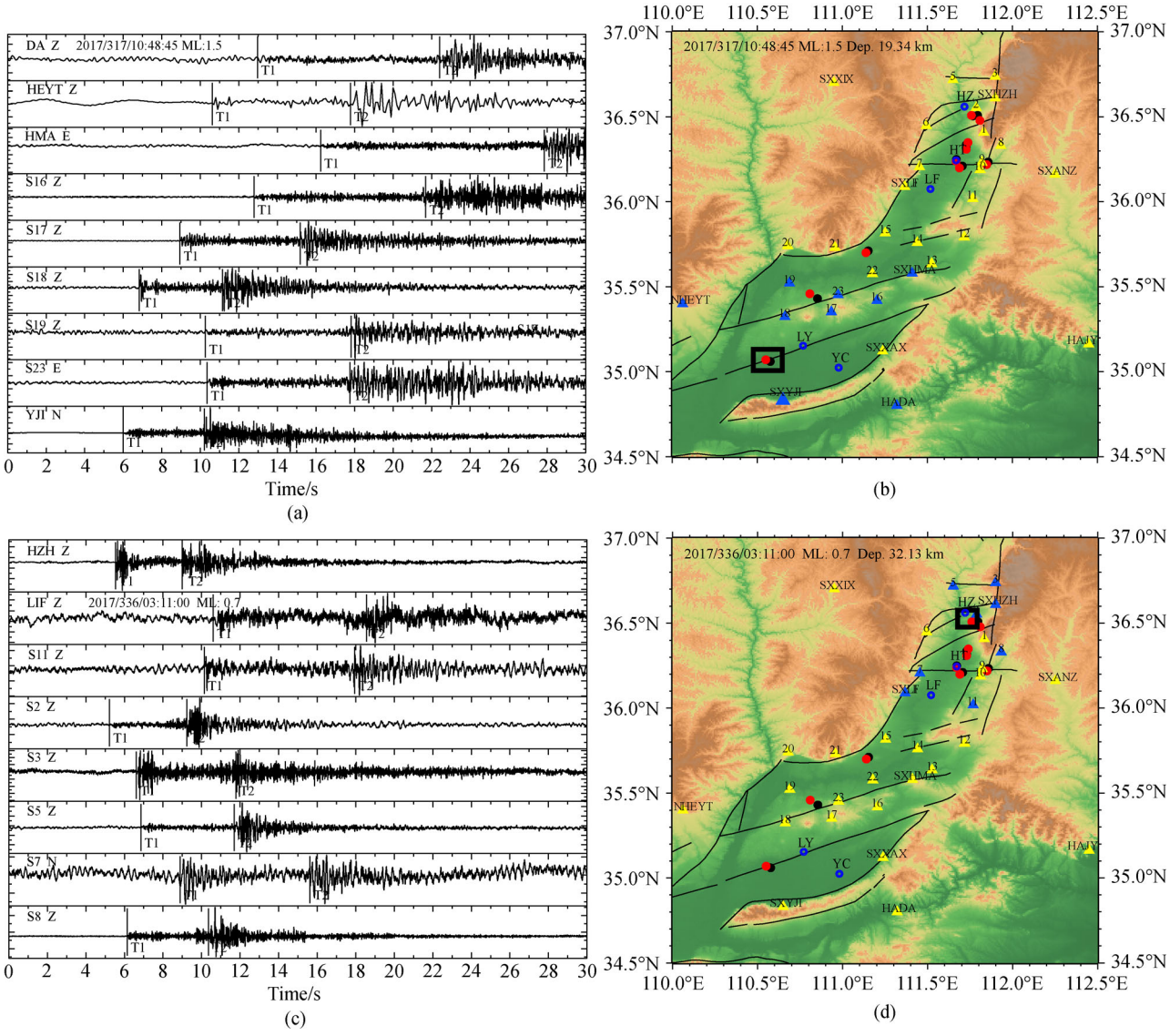

Fig. 7 Waveforms (a, c) and station distribution (blue triangles in b, d) for two typical relocated earthquakes (black boxes in b, d) in the Linfen rift. Red and black dots (b, d) show the seismic events before and after relocation.

containing most of the ten new events in the study, was distributed along the profile in the Linfen rift and corresponded to the high-conductivity materials observed by magnetotelluric sounding (Yin et al., 2017). An uneven high-velocity zone with a depth between 12 km and 18 km was detected along the profile, corresponding to high-resistivity materials observed by the magnetotelluric sounding (Yin et al., 2017). The magnitude 7.75 earthquake in LF in 1695 CE occurred in the interior of a high-velocity body, while the magnitude 8.0 earthquake that struck HT in 1303 CE occurred at the bottom (Fig. 8(c)). These results suggest that these two earthquakes occurred in an environment of high-strength rock.

The earthquakes in the Linfen rift zone were primarily distributed in the upper-middle crust, with a focal depth of less than 35 km (Fig. 8), suggesting the range of the seismogenic layer. Local lower-velocity zones were imaged in the middle-lower crust by the joint inversion (Figs. 5 and 8). The lower velocity anomaly was observed from the uppermost mantle to a depth greater than 300 km. However, based on our study and previous surface wave and body-wave tomography analysis (Zhao et al., 2009; Tang et al., 2013; Shen et al., 2016; Ling et al., 2017). it was absent from the bottom of the seismogenic layer to the uppermost mantle.

This phenomenon suggests that the upwelling materials should not have affected the velocity structure between the bottom of the seismogenic layer to the uppermost mantle (Fig. 9). In addition, the heat contributed by the upwelling mantle did not appear to affect the crust due to its general

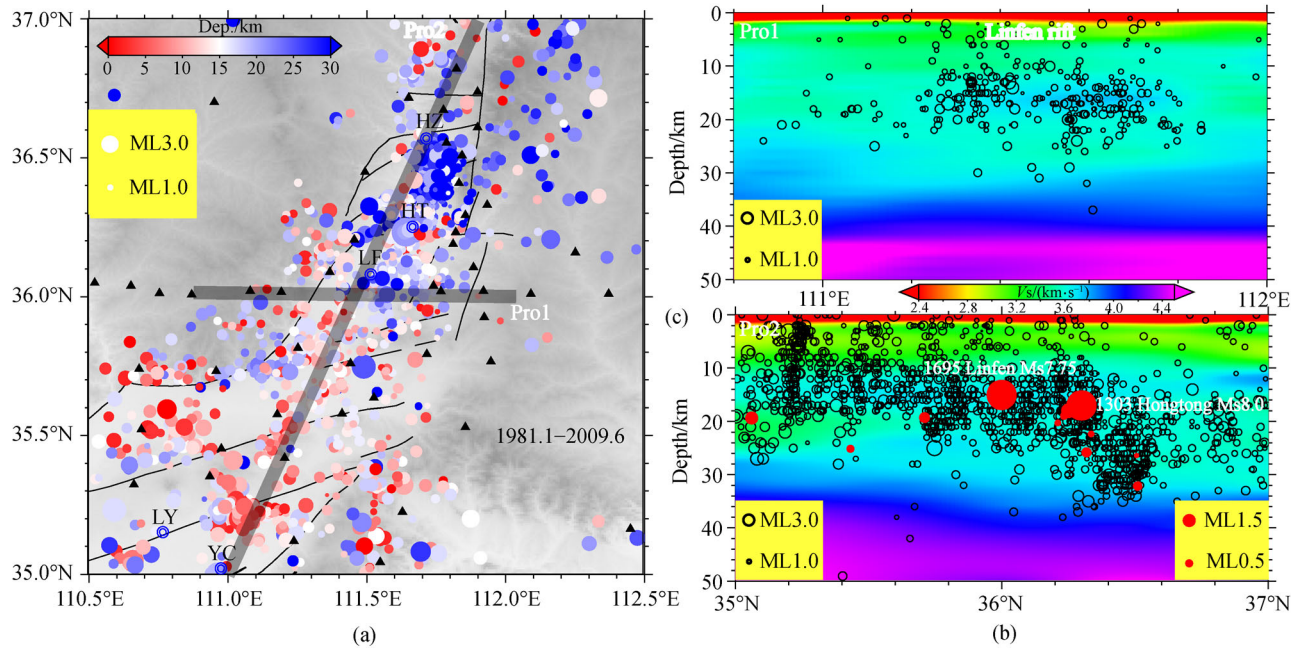

Fig. 8 The earthquake distribution from January 1981 to June 2009 and S-wave velocity beneath two profiles in the study region. The 20 km radius earthquakes are projected in b; all earthquakes projected in c. Red solid circles (c) show the locations of the ten relocated deep earthquakes and two strong earthquakes. HZ: Huozhou City; HT: Hongtong City; LF: Linfen City; LY: Linyi City; YC: Yuncheng City.

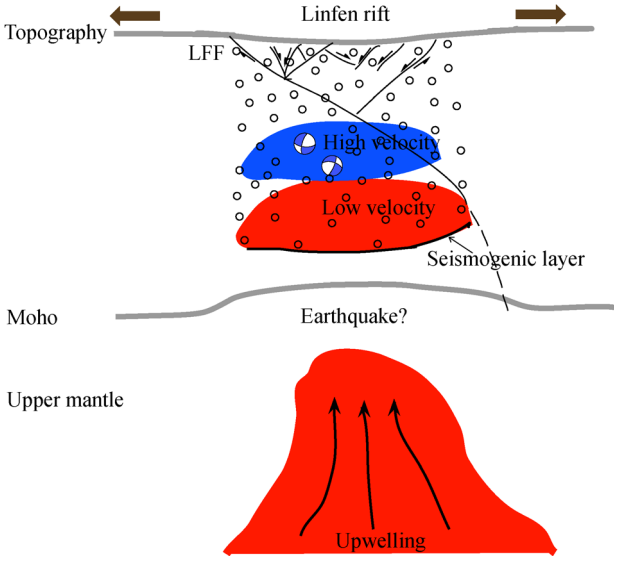

Fig. 9 A profile sketch of the present velocity results and additional mantle tomography results and seismicity in the Linfen rift. Black arrows show the directions of stretching force and circles show the earthquakes. LFF:Linfen–Fushan fault. Circles show the earthquakes. The focal spheres show the Linfen Ms 7.75 (1695) and Hongtong Ms 8.0 (1303) earthquakes.

brittle failure based on the distribution of seismicity (Fig. 8). Our results do not support the views that crustal-scale faults exist, nor the occurance of earthquakes in the mantle in the Linfen rift zone.

4 Conclusions

Using teleseismic waveform data from 27 broadband seismic stations and phase velocity dispersion curves, we obtained the S-wave velocities from the surface to a depth of 70 km in the Linfen rift and its surroundings using the joint inversion of a receiver function and surface wave dispersion. Based on the crustal velocity structure and waveform records collected at 23 densely spaced, temporary stations, we relocated the source parameters for ten events from depths > 20 km in the Linfen rift zone. By comparing and analyzing the relationship between crustal S-wave velocity and seismic activity, we arrived at four main conclusions:

1) Lateral changes of S-velocity at different depths were imaged in the Linfen rift zone and clear differences in S-wave velocities were observed between the Linfen rift and the surrounding mountains at some depths. Local lower-velocity zones were observed in the middle-lower crust, but none were detected from the bottom of the seismogenic layer to the uppermost mantle.

2) The focal depth of most relocated earthquakes was between 18 km and 26 km. One relocated earthquake had a focal depth of 32 km in the lower crust of the Linfen rift zone.

3) Most of the relocated earthquakes occurred in a lower-velocity zone with depths from 18 km to 34 km. The historic earthquakes of LF (magnitude 7.75) and HT (magnitude 8.0) occurred in the interior and at the bottom of the high-velocity zone with depths from 12 km to 18 km, respectively.

4) The upwelling mantle materials have yet to remarkably affect the velocity structure between the seismogenic layer and the uppermost mantle, or to heat the crust given its general brittle failure based on the distribution of seismicity. Crustal-scale faults may not exist, and earthquakes may not occur in the mantle in the Linfen rift zone.

Acknowledgements We are thankful to the Seismic Array Laboratory, Institute of Geology and Geophysics, Chinese Academy of Sciences (doi:10.12129/IGGSL.Data.Observation, available at Seislab website) and Data Management Centre of China National Seismic Network at Institute of Geophysics (SEISDMC, doi:10.11998/SeisDmc/SN), China Earthquake Networks Center and SX Seismic Networks, China Earthquake Administration, for providing seismic data of temporary and permanent stations, respectively. We thank Xing Wei and Yonghong Duan for the earthquake data and the P-wave velocity model in the Linfen rift, respectively. We thank Sidao Ni for beneficial discussions. We also thank editors and two anonymous reviewers for their constructive reviews. This work is supported by the DREAM Project of the National Key R&D Program of China (No. 2016YFC0600402) and the National Natural Science Foundation of China (Grant No. 41604056).

References

Bao X W, Song X D, Xu M J, Wang L S, Sun X X, Mi N, Yu D Y, Li H (2013). Crust and upper mantle structure of the North China Craton and the NE Tibetan Plateau and its tectonic implications. Earth Planet Sci Lett, 369: 129–137

Cai Y, Jian-Ping W U, Fang L H, Wang W L, Huang J (2014). Relocation of the earthquakes in the eastern margin of Ordos block and their tectonic implication in the transition zones of extensional basin. Chin J Geophys, 57(4): 1079–1090 (in Chinese)

Chen L, Jiang M M, Yang J H, Wei Z G, Liu C Z, Ling Y (2014). Presence of an intralithospheric discontinuity in the central and western North China Craton: implications for destruction of the craton. Geology, 42(3): 223–226

Chen W P, Yang Z (2004). Earthquakes beneath the Himalayas and Tibet: evidence for strong lithospheric mantle. Science, 304(5679): 1949–1952

Chu R S, Helmberger D V, Sun D Y, Jackson J M, Zhu L (2010). Mushy magma beneath Yellowstone. Geophys Res Lett, 37(1): L01306

Ding Z F, Zeng R S (1990). A preliminary study of focal depth distribution in the Beijing-Tianjin-Tangshan. Acta Seismol Sin, 12(3): 242–247 (in Chinese)

Dong C L, Li L, Zhao J Q, Li D M, Hu Y L, Ren L W, Xu Z G (2013). Relocation of small earthquakes in Linfen area, Shanxi, China. Seismology and Egeology, 35(4): 873–886 (in Chinese)

Duan Y H, Wang F Y, Zhang X K, Lin J Y, Liu Z, Liu B F, Yang Z X, Guo W B, Wei Y H (2016). Three dimensional crustal velocity structure model of the middle-eastern North China Craton (HBCrust1.0). Sci China Earth Sci, 59(7): 1477–1488

Feng M, An M J, Dong S W (2017). Tectonic history of the Ordos Block and Qinling Orogen inferred from crustal thickness. Geophys J Int, 210(1): 303–320

Gao M (1995). Study on the seismogenic tectonics of 1695 Linfen Macroquake. Earthquake Research in Shanxi, 3–4: 24–28 (in Chinese)

Herrmann R B (2013). Computer programs in seismology: an evolving tool for instruction and research. Seismol Res Lett, 84(6): 1081–1088

Hu J F, Zhu X G, Xia J Y, Chen Y (2005). Using Surface wave and receiver function to jointly inverse the crust-mantle velocity structure in the west Yunnan area. Chin J Geophys, 48(5): 1148–1155 (in Chinese)

Hu X L, Dian G L, Gao J C, Chuai Y Q, Duan Y R, Zhang Y Q, Li X Y, Jian C L, Mi X M (2002). The redetermination of hypocentral location for present earthquakes in Hongtong and Linfen area, Shanxi province. North China Earthguake Sciences, 20(2): 10–15 (in Chinese)

Hu S B, He L J, Wang J Y (2000). Heat flow in the continental area of China: a new data set. Earth Planet Sci Lett, 179(2): 407–419

Jiang M M, Ai Y S, Chen L, Wang Y J (2013). Local modification of the lithosphere beneath the central and western North China Craton: 3D constraints from Rayleigh wave tomography. Gondwana Res, 24(3-4): 849–864

Jiang M M, Zhou S Y, Tong X P, Liang X F, Chen Y S (2009). Accurate depth determination of deep earthquake in southern Tibet and its geodynamic implication. Chin J Geophys, 52(9): 2237–2244 (in Chinese)

Jin Y K, Fan J, Zhao H M, Song M Q, Zhang L, Dong C L (2008). Preliminary application of double difference earthquake locating method for more accurate locating small medium earthquakes in Shanxi. Earthquake Research in Shanxi, 4: 11–14 (in Chinese)

Julià J, Ammon C J, Herrmann R B, Correig A M (2000). Joint inversion of receiver function and surface wave dispersion observations. Geophys J R Astron Soc, 143(1): 99–112

Klein F W (2007). User's Guide to HYPOINVERSE-2000, a FORTRAN Program to Solve for Earthquake Location and Magnitude, version1.40. U.S. Geol Surv. Open File Rep: 02–171

Langston C A (1977). Corvallis, Oregon, crustal and upper mantle structure from teleseismic P and S waves. Bull Seism Soc Am, 67: 713–724

Laske G, Masters G, Ma Z (2013). Update on CRUST1.0- A 1-degree global model of earth's crust. In: EGU General Assembly Conference Abstracts

Li B, Sørensen M B, Atakan K (2015a). Coulomb stress evolution in the Shanxi rift system, North China, since 1303 associated with coseismic, post-seismic and interseismic deformation. Geophys J Int, 203(3): 1642–1664

Li D, Zhou S Y, Chen Y S, Feng Y G, Li P (2012). 3-D lithospheric structure of upper mantle beneath Ordos region from Rayleigh-wave tomography. Chin J Geophys, 55(5): 1613–1623 (in Chinese)

Li S L, Mooney W D, Fan J C (2006). Crustal structure of China's mainland from deep seismic sounding data. Tectonophysics, 420(1–2): 239–252

Li Y H, Gao M T, Wu Q J (2014a). Crustal thickness map of the Chinese mainland from teleseismic receiver functions. Tectonophysics, 611: 51–60

Li Z H, Liu B J, Yuan H K, Feng S Y, Chen W, Li W, Kou K P (2014b). Fine crustal structure and tectonics of Linfen Basin from the results of seismic reflection profile. Chin J Geophys, 57(5): 1487–1497 (in Chinese)

Li Z W, Hao T Y, Xu Y, Xu Y, Roecker S (2010). A global optimizing

approach for waveform inversion of receiver functions. Comput Geosci, 36(7): 871–880

Li Z W, Huang Z B, Wang X X, Han L B (2015b). A study on the reliability of M4~5 earthquakes with anomalous focal depth in the USGS earthquake catalog: several earthquakes in the North-South Seismic Belt. Chin J Geophys, 58(4): 1236–1250 (in Chinese)

Lindenfeld M, Rümpker G (2011). Detection of mantle earthquakes beneath the East African Rift. Geophys J Int, 186(1): 1–5

Ling Y, Chen L, Wei Z G, Jiang M M, Wang X (2017). Crustal S-velocity structure and radial anisotropy beneath the southern part of central and western North China Craton and the adjacent Qilian Orogenic Belt from ambient noise tomography. Sci China Earth Sci, 60(10): 1752–1768

Liu Q Y, van der Hilst R D, Li Y, Yao H J, Chen J H, Guo B, Qi S H, Wang J, Huang H, Li S C (2014). Eastward expansion of the Tibetan Plateau by crustal flow and strain partitioning across faults. Nat Geosci, 7(5): 361–365

Lou X H, Ai Y S, Zhang Y Y, Chen Y S, Ning J Y (2017). Study of lithospheric structure in the central and western North China craton. Prog Geophys, 32(4): 1458–1464 (in Chinese)

Ma J, Feng X J, Li G Y, Li X N, Zhang Y (2016). The coseismic vertical displacements of surface rupture zone of the 1556 Huaxian earthquake. Seismology and Egeology, 38(1): 22–30 (in Chinese)

Ma Z J (1993). Linfen Region Seismic Study, Earthquake Pre-evaluation and Prevention, Shanxi. Beijing: Earthquake Press

Mori (1991). Estimates of velocity structure and source depth using multiple P waves from aftershocks of the 1987 Elmore Ranch and Superstition Hills, California, earthquakes. Bull Seism Soc Am, 81(2): 508–523

Radziminovich N, Balyshev S, Golubev V (2003). Earthquake focal depths and crustal strength in the Baikal rift. Geol Geofiz, 44(11): 1214–1223 (in Russian)

Ren X, Xu Z G, Yang H, Chen H F, Zou L H (2012). Moho depth distribution character beneath the Ordos block's southeastern margin areas. Chin J Geophys, 55(12): 4089–4096 (in Chinese)

Shapiro N M, Campillo M (2004). Emergence of broadband Rayleigh waves from correlations of the ambient seismic noise. Geophys Res Lett, 31(7): L07614

Shen W S, Ritzwoller M H, Kang D, Kim Y H, Lin F C, Ning J Y, Wang W T, Zheng Y, Zhou L Q (2016). A seismic reference model for the crust and uppermost mantle beneath China from surface wave dispersion. Geophys J Int, 206(2): 954–979

Shen Z K, Wan Y G, Gan W J, Li T M, Zeng Y H (2004). Crustal stress evolution of the last 700 years in North China and earthquake occurrence. Earthquake Res China, 20(3): 211–228 (in Chinese)

Si S K, Tian X B, Zhang H S, Teng J W (2013). Prevalent thickening and local thinning of the mantle transition zone beneath the Baikal rift zone and its dynamic implications. Sci China Earth Sci, 56(1): 31–42

Song M Q, Zheng Y, Ge C, Li B (2012). Relocation of small to moderate earthquakes in Shanxi Province and its relation to the seismogenic structures. Chin J Geophys, 55(2): 513–525 (in Chinese)

Tang Y C, Feng Y G, Chen Y J, Zhou S Y, Ning J Y, Wei S Q, Li P, Yu C Q, Fan W Y, Wang H Y (2010). Receiver function analysis at Shanxi Rift. Chin J Geophys, 53(9): 2102–2109 (in Chinese)

Tang Y C, Chen Y S, Zhou S Y, Ning J Y, Ding Z (2013). Lithosphere structure and thickness beneath the North China Craton from joint inversion of ambient noise and surface wave tomography. J Geophys Res Solid Earth, 118(5): 2333–2346

Wang P D (2000). Active faults of the Datong Earthquakes of October 1989 and March 1991. Seismological & Geomagnetic Observation & Research, 21(6): 19–26 (in Chinese)

Wei Z G, Chen L, Wang B Y (2013). Regional variations in crustal thickness and Vp/Vs ratio beneath the central-western North China Craton and adjacent regions. Geol J, 48(5): 531–542

Wei Z G, Chu R S, Chen L (2015a). Regional differences in crustal structure of the North China Craton from receiver functions. Sci China Earth Sci, 58(12): 2200–2210

Wei Z G, Chen L, Jiang M M, Ling Y (2015b). Lithospheric structure beneath the central and western North China Craton and the adjacent Qilian orogenic belt from Rayleigh wave dispersion analysis. Tectonophysics, 646: 130–140

Wei Z G, Chen L, Li Z W, Ling Y, Li J (2016). Regional variation in Moho depth and Poisson's ratio beneath eastern China and its tectonic implications. J Asian Earth Sci, 115: 308–320

Wei S J, Ni S D, Chong J J, Zheng Y, Chen Y (2009). The 16 August 2003 Chifeng earthquake: is it a lower crust earthquake? Chin J Geophys, 52(1): 111–119 (in Chinese)

Wolfe C J, Okubo P G, Shearer P M (2003). Mantle fault zone beneath Kilauea Volcano, Hawaii. Science, 300(5618): 478–480

Wu Q J, Zeng R S (1998). The crustal structure of Qinghai-Tibet plateau inferred from broadband teleseismic waveform. Chin J Geophys, 41 (5): 669–679 (in Chinese)

Xi G J, Zhang C G (1977). Shanxi rift and earthquakes. Earthquake Research in Shanxi, 4: 20–24 (in Chinese)

Xu X, Ma X, Deng Q (1993). Neotectonic activity along the Shanxi rift system, China. Tectonophysics, 219(4): 305–325

Xu Y R, He H L, Deng Q D, Allen M B, Sun H, Bi L S (2018). The CE 1303 Hongdong earthquake and the Huoshan Piedmont Fault, Shanxi Graben: implications for magnitude limits of normal fault earthquakes. J Geophys Res Solid Earth, 123(4): 3098–3121

Yang Z X, Chen Y T, Zheng Y J, Yu X W (2003). Accurate relocation of earthquakes in central-western China using the double-difference earthquake location algorithm. Science in China, 33(S1): 129–134 (in Chinese)

Yao H J, Van Der Hilst R D, De Hoop M V (2006). Surface-wave array tomography in SE Tibet from ambient seismic noise and two-station analysis-I. Phase velocity maps. Geophys J Int, 166(2): 732–744

Yin Y T, Jin S, Wei W B, Ye G F, Jing J, Zhang L, Dong H, Xie C, Liang H (2017). Lithospheric rheological heterogeneity across an intraplate rift basin (Linfen Basin, North China) constrained from magnetotelluric data: implications for seismicity and rift evolution. Tectonophysics, 717: 1–15

Zandt G, Ammon C J (1995). Continental crust composition constrained by measurements of crustal Poisson's ratio. Nature, 374(6518): 152–154

Zhang Y Q, Ma Y S, Yang N, Shi W, Dong S W (2003). Cenozoic extensional stress evolution in North China. J Geodyn, 36(5): 591–613

Zhao L, Allen R M, Zheng T Y, Hung S H (2009). Reactivation of an Archean craton: constraints from P- and S-wave tomography in North China. Geophys Res Lett, 36(17): L17306

Zheng X F, Yao Z X, Liang J H, Zheng J (2010). The role played and opportunities provided by IGP DMC of China National Seismic Network in Wenchuan earthquake disaster relief and researches. Bull Seismol Soc Am, 100(5B): 2866–2872

Zheng Y, Xie Z (2017). Present status and prospect of earthquake focal depth locating. Journal of Seismological Research, 40(2): 167–175 (in Chinese)

Zhu A L, Xu X W, Zhou Y S, Yin J Y, Gan W J, Chen G H (2005). Relocation of small earthquakes in Western sichuan, China and its implications for active tectonics. Chin J Geophys, 48(3): 692–700 (in Chinese)

Zhu L P, Helmberger D V (1996). Intermediate depth earthquake beneath the India-Tibet collision zone. Geophys Res Lett, 23(5): 435–438